

Review

A Review on Solid-State-Based Additive Friction Stir Deposition

Hongrui Dong¹, Xiaoqiang Li^{2,*}, Ke Xu², Zhenyu Zang², Xin Liu², Zongjiang Zhang², Wenlong Xiao¹ and Yong Li²

¹ School of Materials Science and Engineering, Beihang University, Beijing 100191, China

² School of Mechanical Engineering and Automation, Beihang University, Beijing 100191, China

* Correspondence: lixiaoqiang@buaa.edu.cn

Abstract: Additive manufacturing (AM) is an important technology in Industry 4.0. In recent years, solid-state-based additive friction stir deposition (AFSD) has attracted much attention, as it can avoid the inherent defect of melting and rapid solidification in electron beam-based or laser-based AM technologies. The macro and micro laws, finite element simulation, and engineering application technology of the AFSD process are still in their early stages. This paper mainly reviews the equipment, mechanism, the effect of process parameters on macro/micro characters, and the engineering applications of the AFSD process. Further, based on the complex loading conditions during the AFSD process, some perspectives are proposed, including the characterization method, unified constitutive model, novel composite manufacturing technology, and systematic study of the AFSD process.

Keywords: AFSD; dynamic recrystallization; mechanical property



Citation: Dong, H.; Li, X.; Xu, K.; Zang, Z.; Liu, X.; Zhang, Z.; Xiao, W.; Li, Y. A Review on Solid-State-Based Additive Friction Stir Deposition. *Aerospace* **2022**, *9*, 565. <https://doi.org/10.3390/aerospace9100565>

Academic Editor: Khamis Essa

Received: 29 August 2022

Accepted: 23 September 2022

Published: 29 September 2022

Publisher's Note: MDPI stays neutral with regard to jurisdictional claims in published maps and institutional affiliations.



Copyright: © 2022 by the authors. Licensee MDPI, Basel, Switzerland. This article is an open access article distributed under the terms and conditions of the Creative Commons Attribution (CC BY) license (<https://creativecommons.org/licenses/by/4.0/>).

1. Introduction

Additive manufacturing (AM) has attracted much attention in the past few decades. AM technology mainly involves the melting of metal powder under the action of an electron beam or a laser [1]. Rapid solidification largely influences the part micro features and mechanical properties [2]. However, it is easy for solidification cracking and porosity to occur due to the nature of rapid solidification, which is a little similar to the casting process [3]. In recent years, the additive friction stir deposition (AFSD) process has attracted much attention as a new solid-state manufacturing method, which is based on the principles of AM and friction stir welding (FSW) [4,5]. During the AFSD process, the interface bond between deposited material and substrate can be formed by the large plastic deformation under elevated temperature, which does not involve the melting process and cause corresponding defects. Meanwhile, equiaxed and fine microstructures [6,7] and wrought-like mechanical properties [8] can be obtained. However, compared with electron beam-based or laser-based AM, the main limitation of AFSD is its low manufacturing accuracy and low flexibility. In addition, there are also hook defects, cavity defects, kissing-bond defects, etc., [9] which are related to the material type, tool size, and process parameters.

With the high deposition rate of the AFSD process, large parts can be quickly manufactured to evaluate new materials and new geometries. Meanwhile, the application of AFSD in aluminum matrix composite [10], material recycling [11], and additive repair [12] fields has been explored preliminarily.

Much research work has been done to study the AFSD process of aluminum alloy, titanium alloy, magnesium alloy [8], steel [13], amongst others. Some literature has reviewed the friction stir AM [14–17] on a macro level, including different friction stir processes, cladding AM based on multilayer sheets, future development strategy, etc. The friction stir additive manufacturing based on powder or feeding rods has more application in

friction stir processes. In addition, the macro and micro evolutions of different materials during the depositing process have similarities and differences. Therefore, this paper tries to summarize the current work on the AFSD process on a specific level, including the equipment, mechanism, experimental study, etc. The AFSD process mentioned in the following sections only includes the depositing process based on powder or feeding rods. Based on the above work, some perspectives of the AFSD process are proposed to support the potential applications of solid-state additive manufacturing.

2. Additive Friction Stir Deposition (AFSD)

AFSD is a rising solid-state deposition manufacturing process, based on the ideas of friction-stir welding technology. In detail, it can be mainly divided into three modes: powder with the non-consumable tool, rod with the non-consumable tool, and consumable tool. Corresponding principles are shown in Figure 1. The main parts include the hollow tool, feeding material, and substrate. For the AFSD process of rods, first, the feeding rod rotates with the tool and is fed toward the substrate. Then, the feeding rod reaches the substrate and causes much friction heating. Next, the softened material fills the space between the tool and substrate. Under the action of friction heating and large plastic deformation, a metallurgical bond forms between the feeding rod and substrate. When the deposition process becomes steady, the tool starts to move according to the designed NC code. Corresponding process parameters consist of the rotational speed and movement velocity of the tool, the feeding material velocity of powder or rod, the tool morphology, etc.

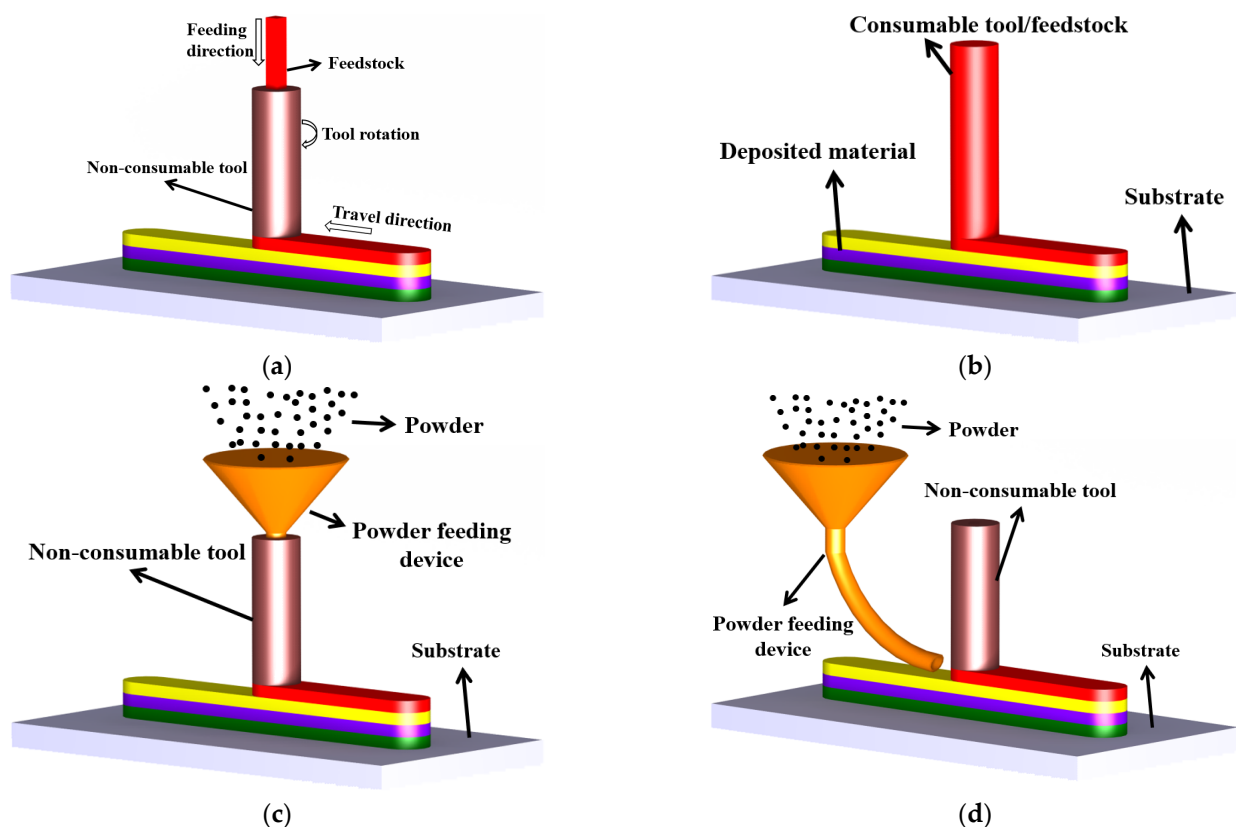


Figure 1. Schematic of the AFSD process with different modes. (a) Rod with non-consumable tool. (b) Consumable tool. (c) Powder with non-consumable tool. (d) Powder with non-consumable tool.

2.1. Equipment and Tool

Different types of equipment are used for the AFSD process, including special and improved machines. For the special equipment used for the AFSD process, MELD (MELD Manufacturing Corporation, Christiansburg VA, USA) has developed different machines

(Figure 2), including K2, L3, B8, and CD-14 systems. Corresponding advantages are shown in Table 1.

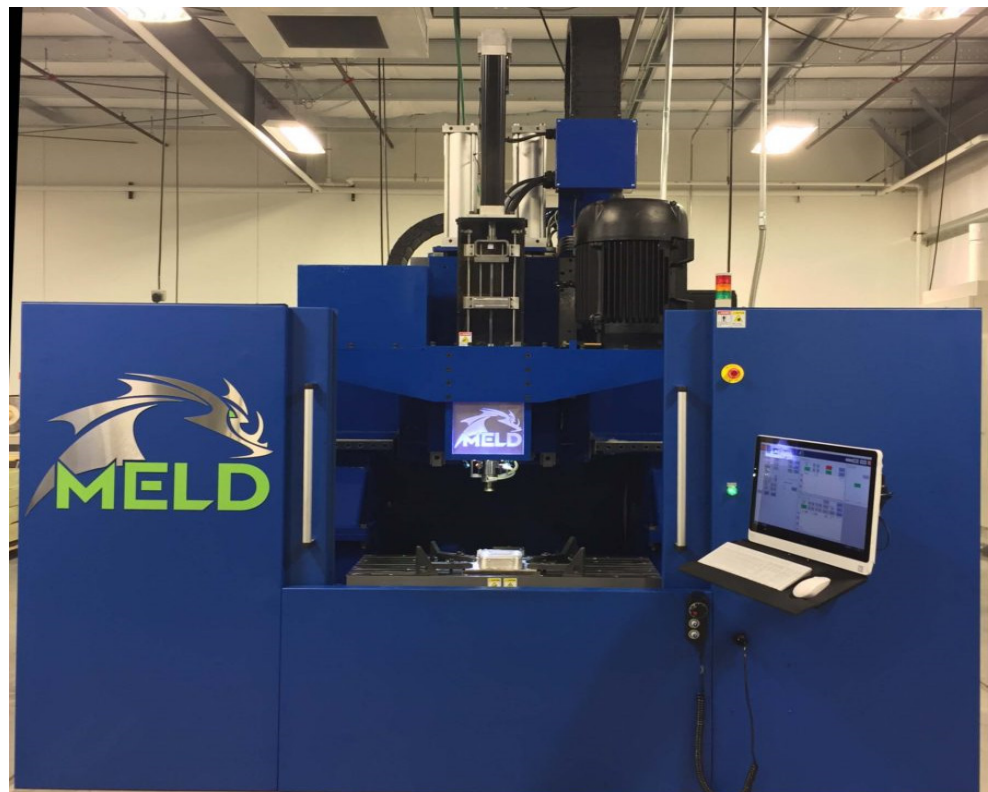


Figure 2. The equipment developed by MELD Corporation [18].

Table 1. The details of different types of equipment.

Machine	Feedstock	Typical Power	Overall Dimension	Advantages
MELD-K2	bar	10–20 A	$6.3 \times 4.66 \times 4.42 \text{ m}^3$	Produce and repair large parts, extreme material flexibility, and low power consumption
MELD-B8	bar	10–20 A	$3 \times 3.35 \times 3.35 \text{ m}^3$	Extreme material flexibility, high material utilization
MELD-L3	bar	10–20 A	$3 \times 2.44 \times 3.96 \text{ m}^3$	Large workspace, increasing production capability
MELD-CD14	bar	10–20 A	$0.8 \times 0.74 \times 2.13 \text{ m}^3$	Integrate the MELD deposition hardware and control system onto an existing machine platform

Besides the above special machines, some types of equipment to operate the AFSD process have been improved, including the FSW machine [19], milling machine [20], and rotary friction welding machine [21]. Some typical improvement methods are shown in Figure 3. In Figure 3a, a consumable rod is fixed by the machine shank of the FSW machine. In Figure 3b, the improved AFSD machine includes a powder duct, a compressor, and a rotational tool. The compressor is used to maintain a stable powder flow. A similar method was also used in the reference [22]. In Figure 3c, the developed AFSD device includes three main parts, namely the powder supply system, powder conveying system, and powder deposition system.

In addition to the machines, the operation tool also plays an essential role in the AFSD process. It limits the geometric boundary of the deposited material in the vertical direction, whereas, in the axial direction, the shear force is applied on the surface of the deposited

material to drive the material flow. Different tools are designed to adapt to different feedstock, mainly including the non-consumable tool with feeding rods, non-consumable tool with feeding powder, and consumable feeding rods, as shown in Figure 1.

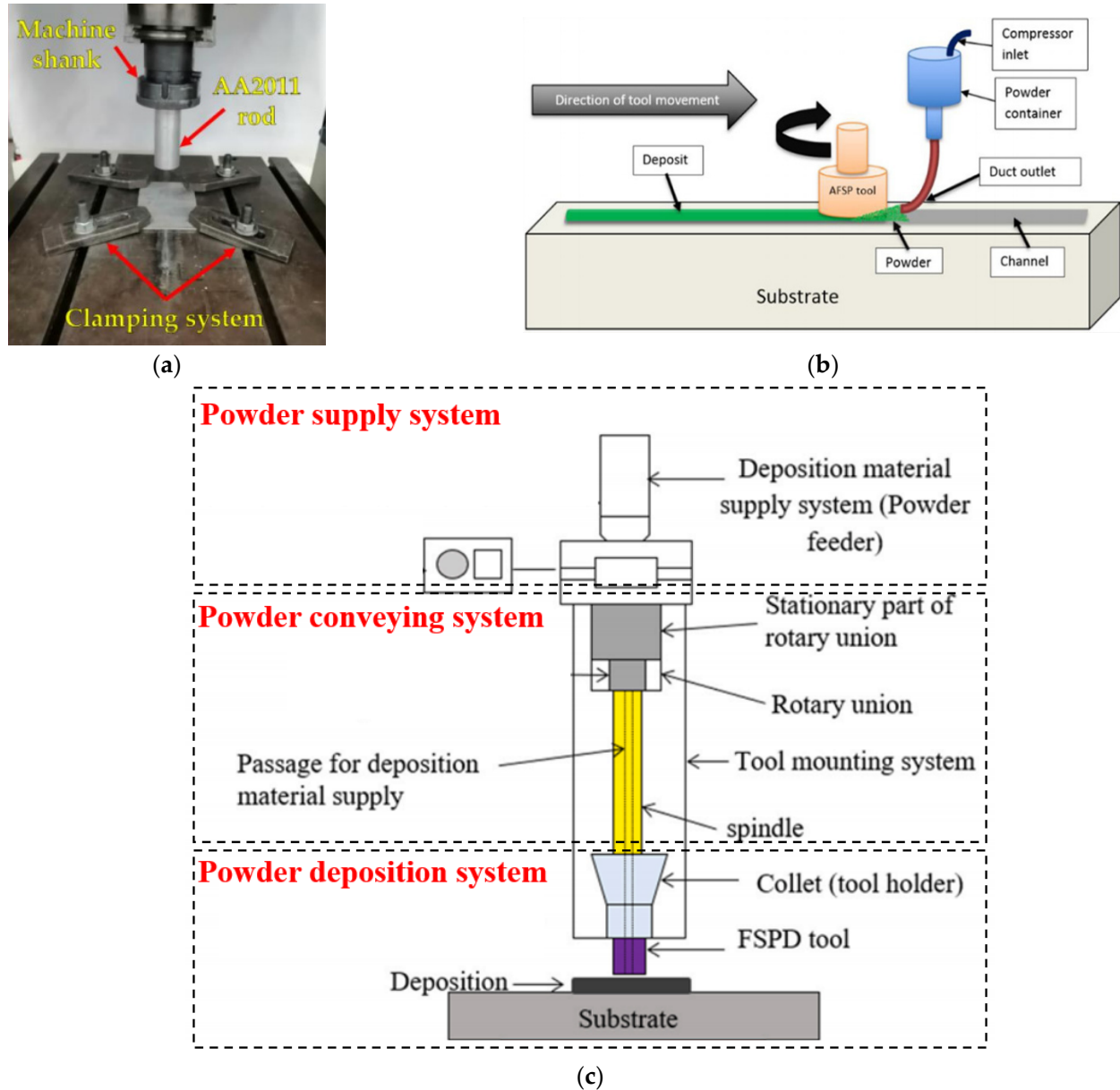


Figure 3. The improved machine used for the AFSD process. (a) The improved FSW machine [23]. (b) The improved machine based on milling machine [20]. (c) Developed apparatus for the AFSD of powder [24].

Different tool morphologies are designed for the non-consumable tool with the feeding rods or powder, mainly including flat and protruding tools, as shown in Figure 4. The protruding tool can cause larger friction heating and plastic deformation, promoting the material flow and mixing between feedstock and substrate. However, it also can cause damage to the surface quality of the deposited layers. Meanwhile, overheating can enlarge the grain size, which can decrease the mechanical properties. Also, the effect of the tool is dependent on the AFSD process parameters.

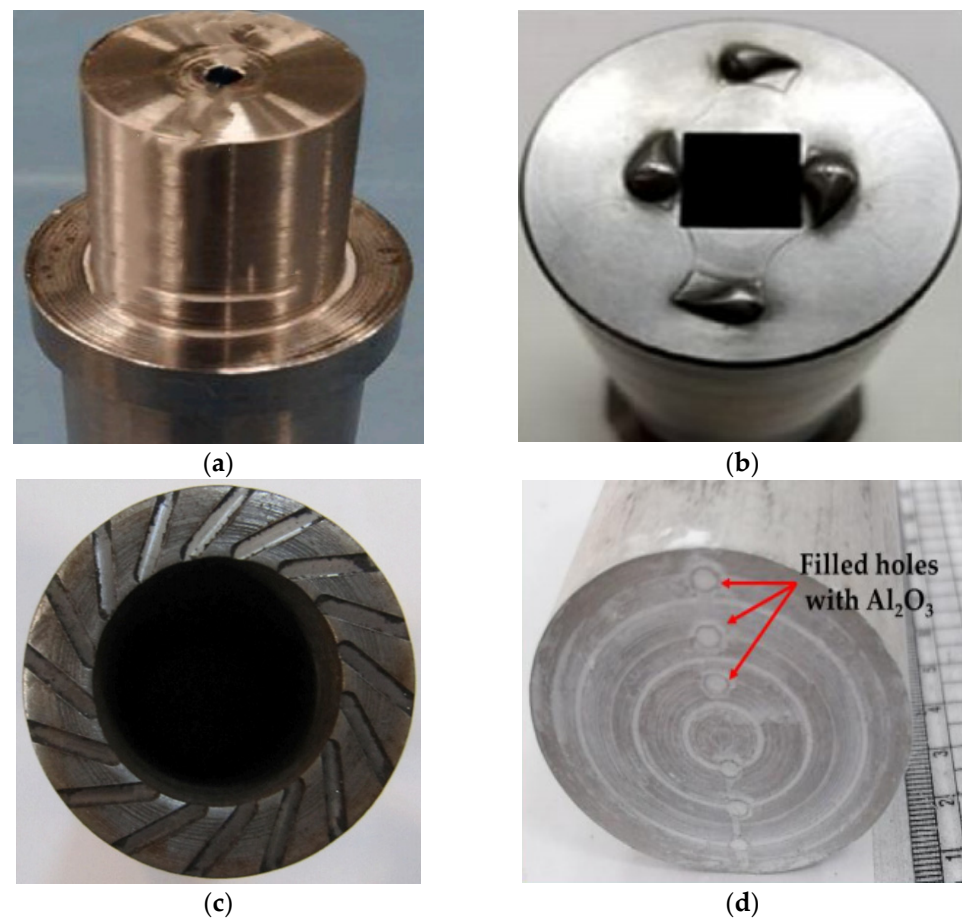


Figure 4. The different tools used for AFSD. (a) Flat tool [24]. (b) Protruding tool with bulges [25]. (c) Friction-forging AM tool [26]. (d) Consumable tool with reinforcing particles [23].

In addition, temperature plays an important role in the AFSD process. However, it is difficult to accurately measure the temperature in real time due to the covered deformation and deposition area. Garcia et al. [27] studied the temperature evolution and heat generation during AFSD of Cu and Al-Mg-Si based on the in-situ method (Figure 5a) and MELD R2 system. Glass fiber insulation tools are used to prevent additional radiation interference. Thermocouples and thermal imagers are used for temperature measurement, and conductive thermal paste is added to improve the response time of temperature measurement. In addition to the above heating source, Chaudhary et al. [22] adopted an extra heating sheet as an external heat source (Figure 5b), which was also used to form a closed-loop temperature-controlled system to maintain the minimum deposition temperature. Moreover, Joshi et al. [28] established a theoretical thermal model based on the multi-layer deposition process of AZ31B, which was verified by the measured temperature with the thermocouple.

2.2. The Mechanism of AFSD

During the AFSD process, feedstock is softened by friction heating and extruded into the space between the tool and substrate. Then, the extruded deposited material is co-deformed and mixed with the surface layer of the substrate to form a strong interface bond. Therefore, the basic deformation mechanism of AFSD is mainly related to temperature and plastic deformation, which affects the deposition quality, microstructure, mechanical property, etc.

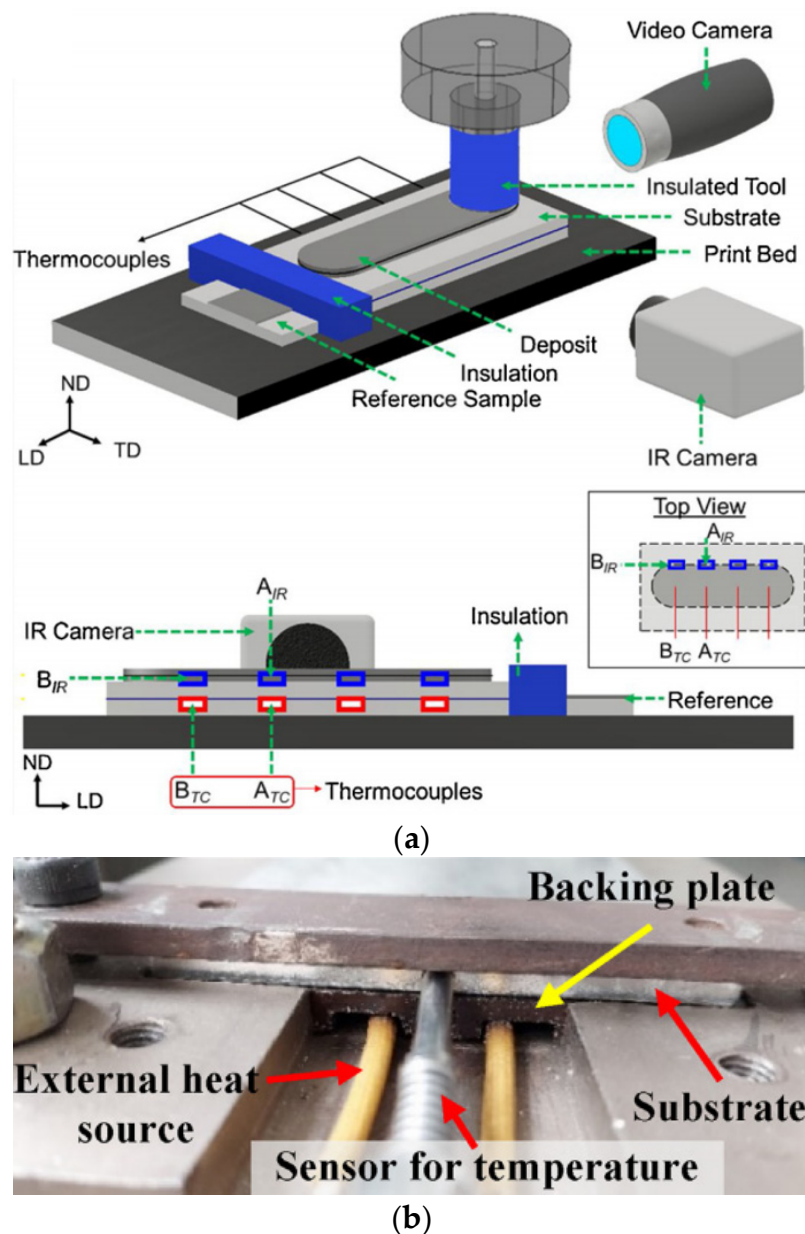


Figure 5. The device for temperature monitoring and extra heating. (a) The designed temperature monitoring device during AFSD. (b) The designed apparatus for the extra heating source.

The heat during the AFSD process includes friction heating and deformation heating. The peak temperature can reach 0.5~0.9 times the melting point [29]. For Al and copper, the peak temperature can be roughly predicted with the equation of $T_{peak}/T_m \approx \text{rotational speed}/\text{travel velocity}$ [27]. To increase the friction heating, additional protrusions are designed on the tool surface to increase the friction heat and enhance the material flow and mixing between the deposit and the substrate. In addition, the deformation heating mechanism varies with the material type. In detail, Garcia et al. [27] found that there was a power law relationship between the peak temperature of Cu and Ω/V , while there was a power law relationship between the peak temperature of Al-Mg-Si and Ω^2/V , which showed that the heat generation mechanism was different for different materials. The above difference was attributed to different interface contact states between the tool and material. The interface contact of Cu was a full slipping state, while the interface contact of Al-Mg-Si was a partial slipping/sticking state. Therefore, friction heating was dominant for Cu, and friction and deformation heatings were dominant for Al-Mg-Si.

Besides the above heating source, the external heat source can promote plastic deformation by improving the minimum temperature value in the AFSD process, which can further improve the deposition quality [22]. In addition, Joshi et al. [28] established a theoretical thermal model based on two parts of energy input, i.e., tool energy and feed energy, which was verified by the deposition process of AZ31B.

The deformation mechanism during the AFSD process mainly includes compression, torsion, and shear deformation path. Perry et al. [30] used the Al-Cu tracer to explore the deformation mechanism of AFSD by embedding tracer material into the Al-Mg-Si matrix (Figure 6). The results showed that the deposited material experienced compression and torsion, then experienced shear-induced thinning. Meanwhile, the total strain could reach 10. In addition, it was revealed that there was significant grain refinement caused by dynamic recrystallization at the initial deposition phase, but no further grain refinement in the steady-state deposition phase.

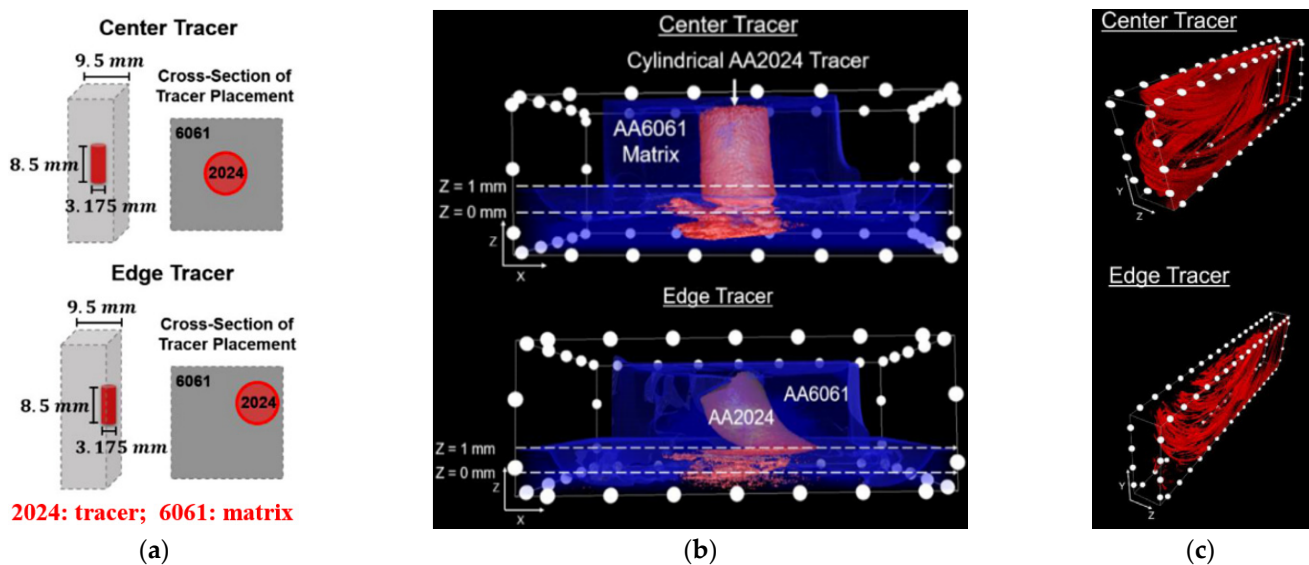


Figure 6. The tracing plastic deformation path method. (a) Schematic of tracer. (b) X-ray tomography after initial feeding. (c) Steady-state deposition.

In addition, the deformation mechanism may vary with the material type. For example, during the AFSD process of Cu, the rotation and flow of the material mainly occur in the transition region, and significant friction heat occurs in the deposition region. During the AFSD process of Al-Mg-Si, the material flows in the deposition area, causing significant shear deformation and generating a large amount of volume heat.

In the process of deposition, temperature and plastic deformation play an important role in the evolution of grain size, and temperature also dominates the influence of plastic deformation. Due to the high temperature and large plastic deformation, dynamic restoration mechanisms occur, such as dynamic recrystallization and dynamic recovery, resulting in fine, equiaxed microstructural features consistent with wrought, rather than cast, materials [31]. The deformation and dynamic recovery make the dislocation accumulate, annihilate, and rearrange, which leads to the formation of sub-grain [32]. Then, the low angle boundary (LAB) and high angle boundary (HAB) form with further deformation. The grain evolution is explained in Figure 7. In detail, the HAB is preserved in areas 1 and 2 due to the small deformation. With the feeding of the rod, the material flows from area 2 to area 3, which experiences large shear deformation and leads to the formation of more LABs. In area 4, grain refinement occurs, and equiaxed grain containing LABs emerges. In area 5, further deformation makes the LABs change to HABs, whose orientation error is larger than 15° .

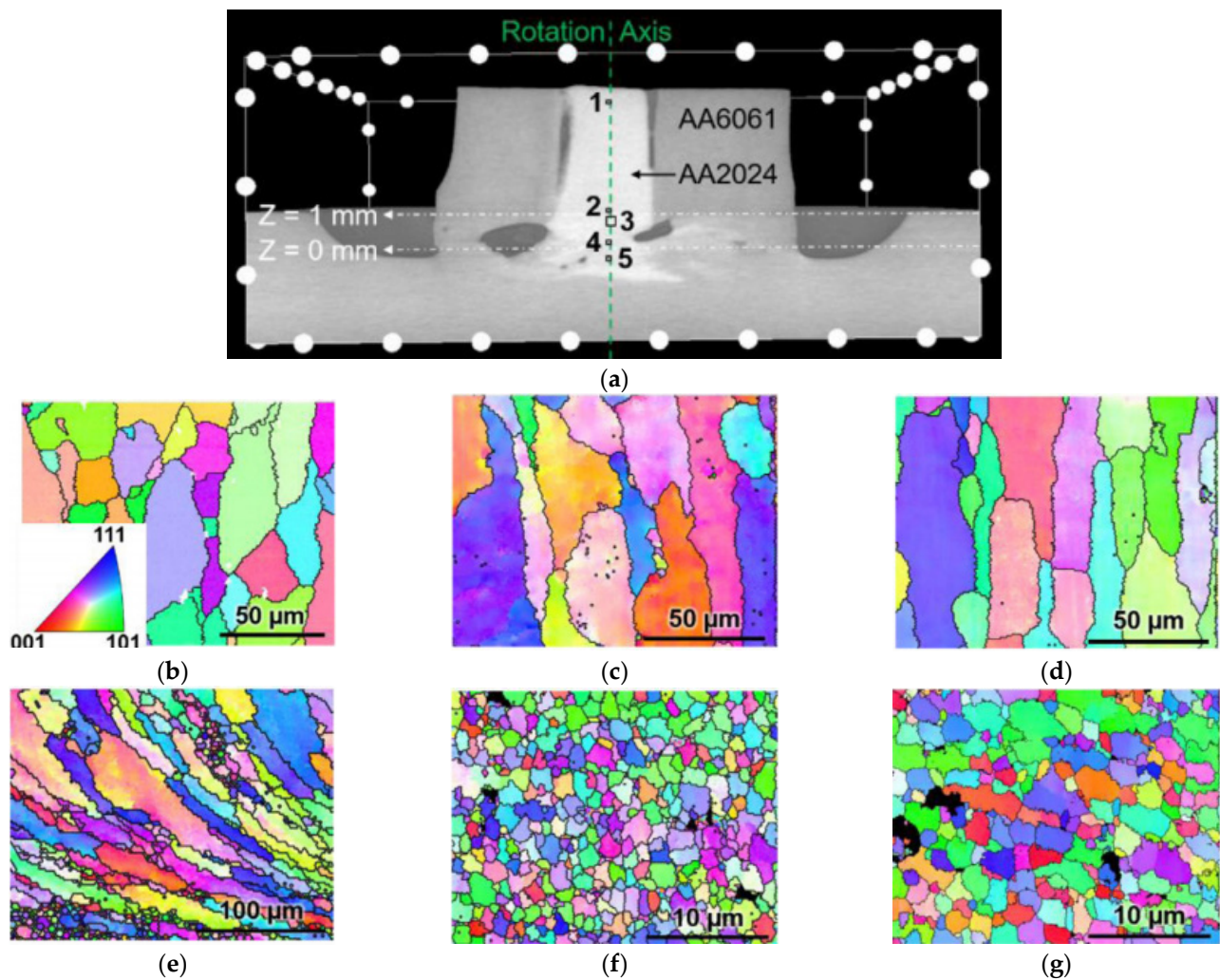


Figure 7. The possible grain evolution at the initial feeding [30]. (a) The cross-section with areas of interest labeled. (b) Base material. (c) Area 1. (d) Area 2. (e) Area 3. (f) Area 4. (g) Area 5.

2.3. The Effect of Process Parameters on Deposition Quality

The most important process parameters during the AFSD process include tool rotational speed, tool travel velocity, and feeding velocity, which influence the deposition temperature and deformation. Some typical rod-base and powder-base AFSD experiments are summarized in Table 2. It can be inferred that most research is focused on the rod-based AFSD process.

Table 2. Some typical rod-base and powder-base AFSD experiments. P: Protruding; F: flat.

Substrate/Deposited Material	Feedstock	Tool	Rotational Speed (rpm)	Feeding Velocity (mm/s)	Travel Velocity (mm/s)	Deposition Thickness Per Layer (mm)	Ref.
6022-T4/6061-T6	Bar	F	300~900	0.85	2.54	0.9	[33]
6022-T4/6061-T6	Bar	P	300~900	1.27	2.54	2.1	[33]
6061-T6/6061-T651	Bar	P	300	1.1	2.12	1	[34]
AZ31B/AZ31B	Bar	F	400	2.1~3.2	4.2~6.3	1	[35]
6061/6061	Bar	P	300	Initial: 0.06 Steady: 0.85	2.54	1	[30]
6061 (P)/6061-T4	Powder	Groove	1200	460mm ³ /min	0.42	0.5	[22]
6061-T6/6061-T651	Bar	P	325	2.1~3.4	1.3	0.5	[36]
6063	Bar	P	300	2.5	4.2	1	[37]
AZ31B-H24/ AZ31B	Bar	F	400	2.1~3.2	4.2~6.3	1	[28]
IN625/HY80	Bar					0.5	[38]
110Cu/110Cu	Bar		275		2.12	1	[39]
Ti6Al4V/ Ti6Al4V	Chip	F	400~500	1.12~1.49	2.54~3.38	0.5	[40]

2.3.1. Surface Quality

The most intuitive characteristic of the deposited part is surface quality, which is affected by the comprehensive impact of tool morphology and process parameters. Hartley et al. [33] studied the effect of tool morphology (flat or protruding tool) and rotational speed (300~900 rpm) on the surface quality based on the solid-state cladding on thin Al-Mg-Si sheet metal under the same tool travel velocity of 2.54 mm/s, as shown in Figure 8. For the flat tool, excellent surface quality could be obtained under 600 rpm with deposition thickness of 0.9 mm per layer. Under 300 rpm, there was slight surface roughness, which was due to insufficient heating and plastic deformation. Under 900 rpm, there were slight surface defects. Therefore, the generated heating should be controlled within a reasonable range, which largely influences the material flow behavior. The surface quality of the protruding tool was worse than that of the flat tool with deposition thickness of 2.1 mm per layer. Due to the existence of bulges, the deposition thickness under the protruding tool was larger than that under the flat tool, which led to lower heating efficiency per unit volume and insufficient material flow.

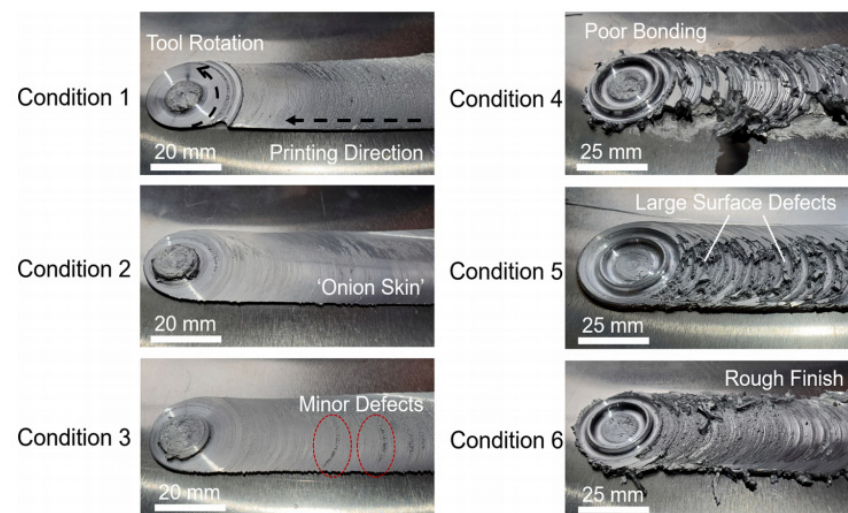


Figure 8. The surface quality of Al-Mg-Si under different conditions. Flat tool: conditions 1~3; Protruding tool: conditions 4~6 [33].

In addition, Joshi et al. [35] found that concentric ripples existed under different process parameters during the AFSD of AZ31B magnesium alloy. During AFSD, there was much friction heating among the tool, substrate, and deposition layer, which softened the feedstock and decreased the flow stress. Meanwhile, the deposition material experienced shear deformation due to the relative motion between the substrate and deposition layer. The heating effect and shear deformation resulted in the formation of ripples. The surface roughness value varied from 9.858 μm to 19.591 μm when the travel velocity varied from 6.3 mm/s to 4.2 mm/s. Under the 4.2 mm/s, more heating was generated and caused the reduction of flow stress, which resulted in more severe plastic deformation and larger roughness. Chaudhary et al. [22] found that using an external heat source can reduce the temperature variation during AFSD and improve the surface quality of the deposition layer, which is due to the uniform temperature and deformation distribution.

It can be inferred that the deposition temperature is the most critical factor for surface quality, which causes a large influence on the material flow. The deposited material can realize sufficient flow under a high heating efficiency per unit volume. In addition, the negative effect of the tool on surface quality can be compensated by the optimized process parameters.

2.3.2. Microstructure

Due to the difference in crystal structure, chemical composition, and strength mechanism, the inherent microstructure evolution during the AFSD process varies with the material type.

For the AFSD of magnesium alloy, such as AZ31B, an α -Mg phase existed in the feedstock and deposition layer. After the AFSD process of AZ31B, the grain size varied from 13.5 μm to 5 μm , which showed that dynamic recrystallization occurred [35]. Meanwhile, the torque variation showed that different slipping systems were activated at different times. However, Joshi et al. [28] found that the grain grew up during the AFSD of AZ31B, whose size varied from the 11 μm of the feeding rod (Figure 9a) to 18 μm of the deposited zone (Figure 9b). The grain size evolutions in the above two papers were opposite. During the AFSD process, the dynamic recrystallization makes the grain fine, while the thermal exposure enlarges it. On a smaller scale, Joshi et al. [28] found that the fraction of precipitate was reduced in the deposited zone, which was attributed to the deformation energy and thermokinetic effect. Moreover, the matrix was in the α -Mg phase, and the precipitate was β phase ($\text{Mg}_{17}\text{Al}_{12}$). In addition, there was no oxide layer detected on the deposition layer due to the slow oxygen diffusion rate under the solid state.

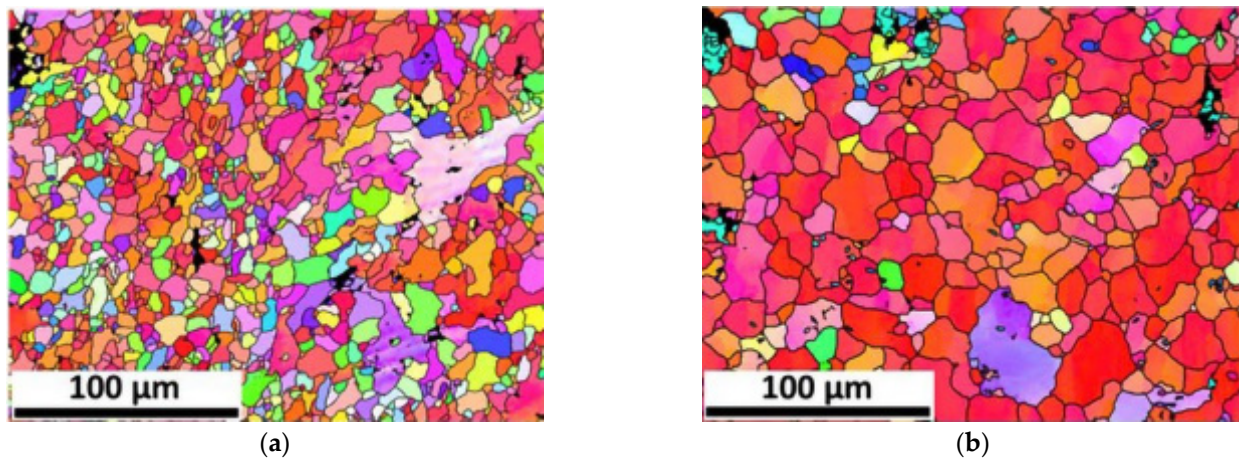


Figure 9. The grain evolution of AZ31B Mg during AFSD process [28]. (a) Initial feedstock (grain size: $11 \pm 3 \mu\text{m}$). (b) After deposition (grain size: $18 \pm 3 \mu\text{m}$).

For the AFSD of copper, Priedeman et al. [39] found that there was surface oxide in the deposition zone (about 1–2 μm) and no obvious interior oxide, which was due to the accumulation of significant oxidation under longer exposure times. Meanwhile, there was very fine porosity at the substrate–deposition interface due to the low initial deposition temperature and rough substrate surface [41], as shown in Figure 10a. Similar to other metal materials, non-uniform grain refinement occurred in the entire deposition zone (Figure 10b). Moreover, there was a positive relationship between the twin density and grain size. Meanwhile, work-hardening was the main strengthening mechanism, and the dislocation density decreased obviously due to the dynamic recrystallization during AFSD of cold-worked Cu, which resulted in the decrease of strength.

For multi-layer deposition of aluminum alloy, there is a refinement of equiaxed grain morphology in the deposited material, as shown in Figure 11. In addition, there is further refinement at the interface between the deposited material and the substrate [42]. However, in some of the literature, it has been found that the grain size in the first layer is larger than that in the other layers due to more thermal recycling in the first layer. For example, the grain size in the third and first deposition layers of 5051-T4 was 6.1 and 9.3 μm , respectively, as shown in Figure 12 [22]. The above two phenomena are opposite, which indicates that the reasonable thermal recycling history may be a useful tool to control grain evolution. In addition, the dissolution and formation of precipitates are also important characteristics

of precipitation-strengthened aluminum alloys. During the AFSD process, the temperature is enough to dissolve the precipitate. Correspondingly, the formation and growth of precipitate are also occurring, which are mainly affected by the process parameters. Therefore, reasonable process parameters are essential to control the microstructure evolution.

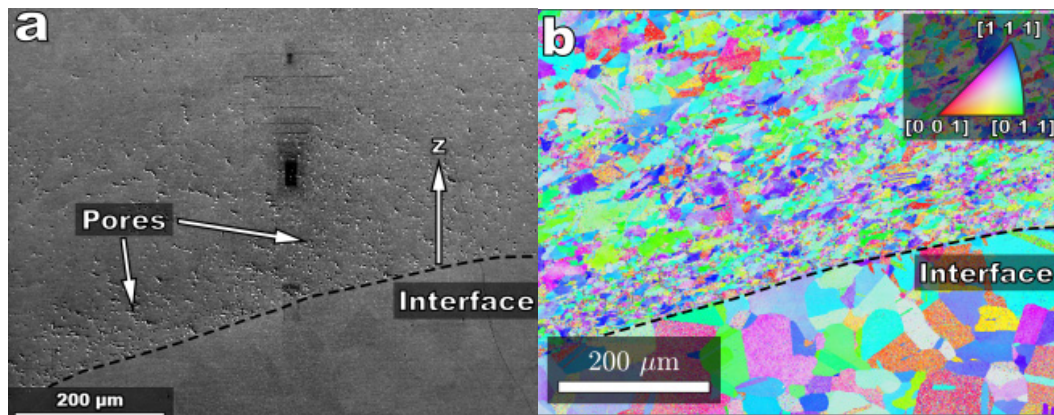


Figure 10. The SEM result of the substrate–deposit interface. (a) Fine porosity at the interface. (b) The inverse pole figure map of the interface.

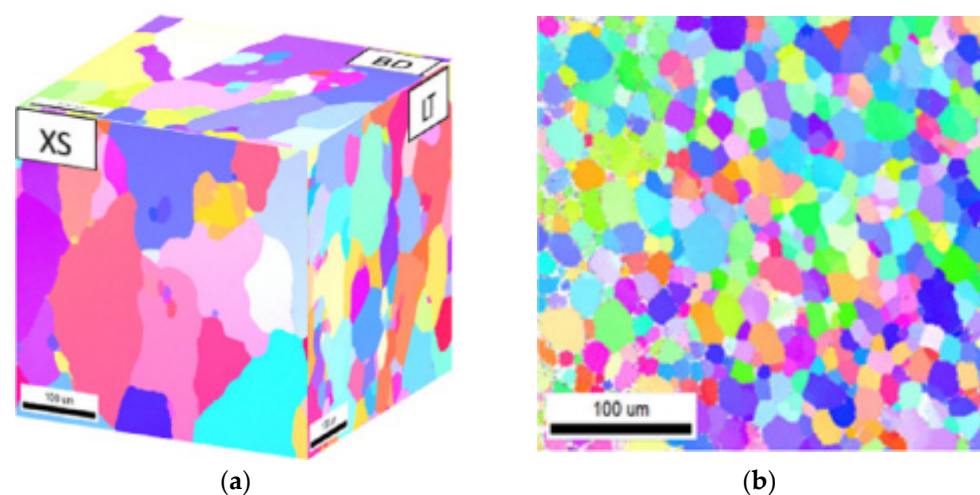


Figure 11. The comparative grain orientation for the feedstock and as-deposited AA6061 [42]. (a) 3-D EBSD map of initial feedstock. (b) EBSD map of deposition cross section.

For the AFSD of Ti6Al4V, Farabi et al. [43] found that dense and homogeneous microstructure could be obtained with the AFSD process. All the samples had transformed α phase, which indicated that the deposition process occurred above the β transition temperature. In addition, compared with melting-based AM, the lower density of the small angle boundary could be obtained with the AFSD process, which meant lower residual stress. Similar findings were also observed in aluminum alloy [44] and Inconel 625 [38]. Moreover, obvious β grain refinement was achieved at a lower temperature, which suppressed the formation of the α grain boundary and achieved higher elongation ($\sim 20\%$).

In summary, dynamic recrystallization is a common characteristic for different materials during the AFSD process due to large plastic deformation and high temperature, which can refine the grain. Meanwhile, it should be noted that high temperatures can promote the grain growth. Therefore, grain evolution is a competitive process of grain refinement and grain growth.

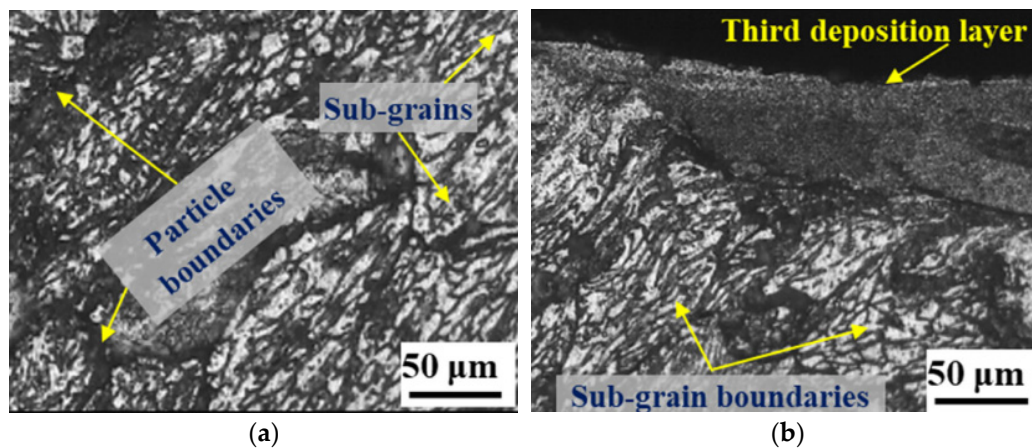


Figure 12. The non-uniform sub-grain distribution at different deposition layers of AA6061. (a) 1st deposition layer (sub-grain size: 9.3 μm). (b) 3rd deposition layer (sub-grain size: 6.1 μm).

2.3.3. Mechanical Properties

With the evolution of grain, composition phase, and precipitate during the AFSD process, the corresponding mechanical properties have different evolution laws for different material, mainly focusing on microhardness and mechanical strength.

Besides the process parameters, the microhardness evolution is also related to the initial heat treatment temper. For example, the initial hardness of AA6061-T6 was 115 ± 10 HV, and the grain size was 110 ± 10 μm . After the deposition, the hardness and grain size becomes 70 ± 6 HV and 20 ± 7 μm , respectively. Theoretically, smaller grain size can increase the material hardness, which is different from the observed result. According to the reference, the MgSi precipitates could be dissolved under the combined actions of high temperature and shear deformation, which resulted in the reduction of hardness [45]. For AA6022-T4, the hardness varies from 81 ± 4 HV to 73 ± 3 HV during AFSD, whose hardness reduction was much smaller than that of AA6061-T6. T4 is the natural aging temper, and T6 is the peaking aging temper. Therefore, the hardness reduction due to precipitate dissolution of T6 temper is larger than that due to precipitate dissolution of T4 temper. Similar results were also found by Phillips et al. [42], Beck et al. [34], and FSW [46]. However, compared with the 6061-T4 substrate, Chaudhary et al. [22] found a small microhardness increase for the deposition of 6061 powder. Therefore, the microhardness evolution of aluminum alloy during AFSD is a multifactorial process. It includes the formation and dissolution of precipitates, grain size evolution, strain-hardening, etc.

In addition, due to the difference in thermal recycling history, there is non-uniform microhardness distribution at the deposition zone. During the AFSD process of AA6061-T6, Kandasamy et al. found that the minimum microhardness value (42HV) was at the first layer, while the maximum microhardness value (58HV) was at the highest layer. Similar hardness gradients were also found in the AA2219 [44], AA7075 [47], 110 Cu alloy [39], etc. As well as the non-uniform microhardness distribution along the vertical direction, it also exists along the tool travel direction. Phillips et al. [48] found that the hardness at the tool head center area was higher than that at the overlapping area, which was attributed to the precipitate dissolution due to repeated heating at the overlapping area.

As for the material strength, different materials have different response behaviors during the AFSD process. In this paper, the material strength variation was categorized according to the material type.

For the magnesium alloy, Robinson et al. [49] found that the yield strength of deposited AZ31B-Mg dropped by 20%, and the ultimate tensile strength (UTS) was the same as that of wrought AZ31B-Mg. The original Mg alloy experienced cold-working, and the dislocations accumulated. During the AFSD, the amount of heat generated caused dislocation annihilation and thus a strength reduction. Williams et al. [50] found that the yield strength

of deposited WE43 Mg dropped by 80 Mpa, UTS dropped by 100 Mpa, and elongation dropped by 11%, which was different from the previous result and related to the original material state.

For aluminum alloy, Martin et al. [36] found that the strength of AA6061-T6 decreased after experiencing the AFSD process. The UTS of AA6061-T6 with deposition experience was higher than that of fusion-base AA6061-T6, but lower than that of initial AA6061-T6. Anderson et al. [51] found that the strength and fatigue life of deposited AA2219 were lower than that of wrought AA2219 under the same strain amplitude. The strength reduction was due to the lack of Al₂Cu phases. The deposited AA2219 accumulated more inelastic damage than the wrought AA2219. However, compared with substrate 5083-H131, the deposited 5083-H131 had lower YS, but higher UTS and elongation, which is similar to the wrought-like mechanical property [11].

For steel, Rivera et al. [38] found that the YS and UTS of deposited Inconel 625 with the AFSD process were higher than that of the cast and wrought Inconel 625, which was attributed to the generated equiaxed grains in three directions. However, there was a light decrease in elongation for deposited Inconel 625. It was found that a crack was propagated through the dynamic recrystallization grain. The results were similar to the FSW of Inconel 625 [52] and Inconel 600 [53]. In addition, the fatigue resistance of deposited Inconel 625 was also improved [54].

For titanium alloy, the YS and UTS of deposited Ti6Al4V could reach 1010 Mpa and 1233 Mpa, respectively [43], which was higher than wrought or melt-based Ti6Al4V. Moreover, a higher elongation (~20%) could be obtained by using a lanthannated-tungsten tool, which had better high-temperature resistance strength and made no tungsten contamination occur. The reduction of deposition temperature decreased the β grain size which improved the mechanical properties.

For metal matrix composite, El-Sayed Seleman et al. [23] compared the mechanical properties of deposited AA2011-O with/without nano Al₂O₃ and AA2011-T6 with/without nano Al₂O₃ composites. The result showed that the compressive strength and wear resistance of deposited composites (AA2011-O/Al₂O₃, AA2011-T6/Al₂O₃) were higher than that of the base material. On the one hand, the Al₂O₃ has high hardness. Meanwhile, the Al₂O₃ can suppress the grain coarsening. Similar results were also found in the AA6061-T6/Al₂O₃ composite [55].

In summary, the severe plastic deformation and friction heating cause dynamic recrystallization, which can improve the hardness of the deposited material through grain refinement. Besides the grain evolution, the precipitate evolution or phase transition may decrease or increase the material strength, which is closely related to the temperature evolution process. Therefore, process parameter control and optimization are very important to achieve property control.

2.3.4. Post-Deposition Heat Treatment

Due to the change in mechanical property after the AFSD process, it is essential to conduct post-deposition heat treatment to improve material performance. Avery et al. [56] conducted heat treatment on the deposited AA7075. The results showed that there was no abnormal grain growth. Meanwhile, the phase Zn-Mg-Cu dissolved, and the precipitates η' and η formed again. Beck et al. [34] studied the effect of post-deposition heat treatment on the micro and macro properties of deposited Al-Mg-Si alloy. The results showed that dynamic recrystallization and grain refinement occurred. Corresponding grain size varied from 100 μm to 20 μm . During the subsequent solid solution process, abnormal grain growth occurred. During the aging following solid solution, abnormal grain growth and refinement occurred simultaneously. The TEM results showed that there was β'' precipitate existing in the initial and aged specimens, while no β'' precipitate existed in the deposited specimen, which indicated that there was precipitate dissolution occurring during AFSD. Babaniaris et al. [37] studied the effect of post-deposition heat treatment (T4, T5, T6) on the microhardness of AA6063, as shown in Figure 13. The uniformly distributed hardness

values could be obtained in T6 due to the solid solutionizing in T6. For the hardness gradient in T4 and T5, it was because the deposited material at the lowest layer experienced multiple thermal recycling, which leads to the consumption of solute atoms due to the precipitation of non-hardening phases.

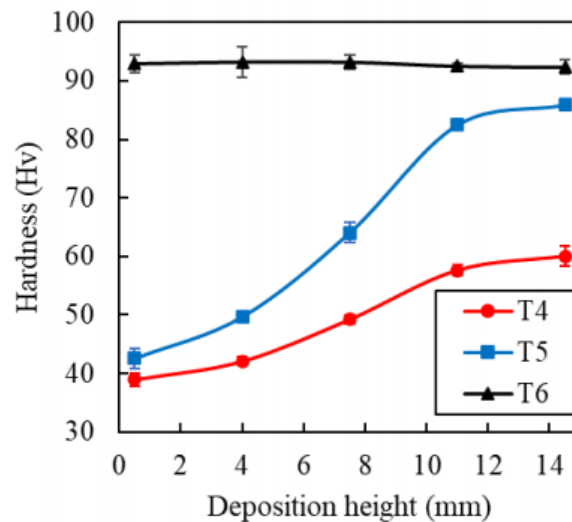


Figure 13. Hardness distribution along the deposition height of AA6063 [37].

Post-heat treatment is an important process, which can cope with the inhomogeneous mechanical property in the deposited part. However, there is still not enough research data revealing the effect of post-deposition heat treatment on deposition material. Further, due to the complex temperature and deformation histories, whether the corresponding heat treatment system is the same as the traditional heat treatment system needs deep study, which is very important for engineering applications of the AFSD process.

3. Simulation

AFSD is a complex thermal–mechanical coupling process with large plastic deformation, which causes difficulty in the corresponding simulation. Numerical simulation is of great importance to elucidate the complex thermodynamic laws and optimize the process parameters.

In general, Lagrangian meshes can accurately describe complex material flow behavior, but they are not as accurate under large deformations. In contrast, Eulerian grids are difficult to predict material flow accurately. Therefore, the coupled Eulerian–Lagrangian method (CEL) can accurately describe the large deformations in the process. Rohatgi [57] used the Lagrangian method to delineate the C3D8RT mesh on H13 tool steel and the Eulerian method to delineate the C3D8RT mesh on a two-layer Al6061 plate substrate. General contact with a friction coefficient of 1.2 was used between the tool and the workpiece, while a pressure-based contact conductivity was selected to simulate the heat transfer from the Al6061 substrate to the base plate. Meanwhile, a low thermal conductivity thin section was set to simulate the heat transfer between the two Al6061 substrates. The error value of the predicted axial force on the tool was only 2% when compared with the experimentally measured axial force.

In addition, many scholars have also adopted a meshless approach to study various dynamic and large deformation problems. Stubblefield et al. [58] adopted a Lagrangian meshless simulation method and smooth particle hydrodynamics (SPH) to simulate a solid-state layer-by-layer incremental stir friction welding process (Figure 14a). Yang et al. [59] modeled the substrate, tool, and feedstock with SPH particles (Figure 14b). Two different convective heat transfer coefficients were also selected for the outer surface of the spindle and substrate in contact with air, and the gap conduction between the substrate and the

feedstock to simulate the heat transfer. The von Mises stress distribution showed significant stress concentrations in the deposition regions. The stress–hardness relationship showed that the top layer of the deposition region had a higher stress value and hardness.

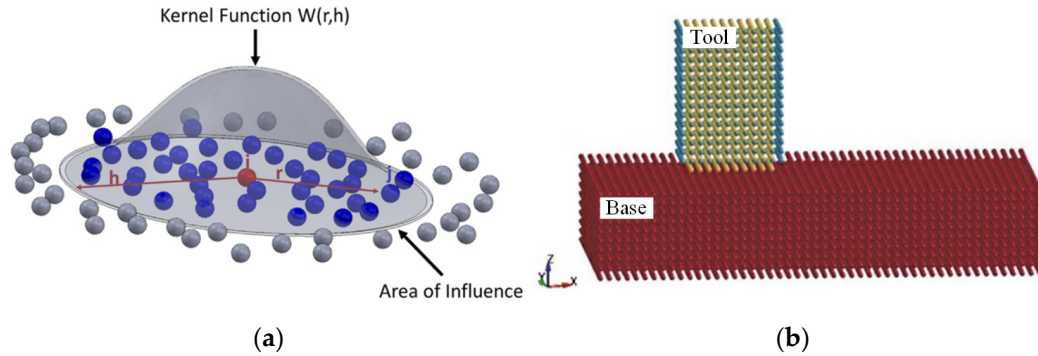


Figure 14. Different types of modeling approaches. (a) SPH of kernel function interpolation. (b) Model with SPH for all components.

Based on the above numerical simulation, the process parameters can be optimized. Stubblefield [60] found that the feeding rate had a significant effect on temperature variation and material properties. More frictional heat was generated at higher feeding rates, which resulted in higher thermal gradients across the part and led to lower residual stresses and/or distortion. In contrast, a low feeding rate was also required to produce a smaller heat-affected zone. In addition, the temperature in the center of the deposition zone was lower than that in the area below the extrusion tool (Figure 15a). There was also a temperature asymmetry between the backward and forward sides of the deposition zone caused by the tool speed and the feedstock used as a heat sink (Figure 15b). In addition, the effective plastic strain analysis showed that lower feeding rates might lead to heterogeneous materials, while higher feeding rates enhanced the material flow and resulted in more homogeneous materials. Lauvray et al. [61] used GMSH software to build a tetrahedral mesh and used the MORFEO solver to investigate the effect of parameters on the rotary frictional heating before deposition. The results showed that the maximum temperature increases linearly with increasing parameters, doubling the rotational speed increasing the maximum temperature reached at the friction interface by a factor of 1.8, and doubling the axial force increasing the maximum temperature by a factor of nearly 2.

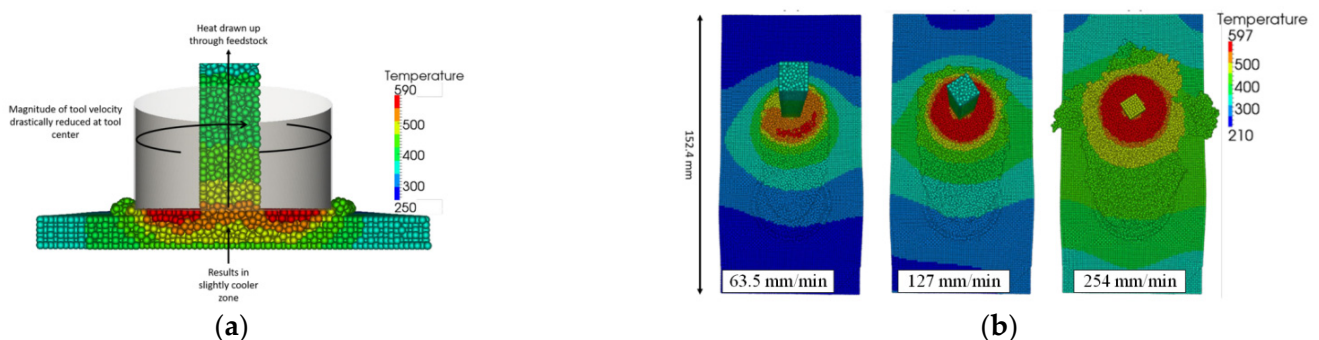


Figure 15. Temperature distribution pattern of AFSD model [60]. (a) Temperature distribution. (b) Temperature asymmetry at three feed rates.

In summary, numerical simulation is an important method to study the deposition mechanism of the AFSD process, including the heating generation mechanism and deformation mechanism.

4. Engineering Application

Compared with fusion-base AM technology, AFSD has higher deposition rates, which makes the AFSD produce, coat, and repair large parts [38]. MELD summarized the deposition rates of different materials, as shown in Table 3.

Table 3. The deposition rates of different materials based on AFSD.

Material	Al	Steel	Ti	Ni
Deposition rate (kg/h)	13.6	4.9	2.5	0.7

AFSD is explored to produce large and fully-dense additive components with minimal residual stress. Some examples are shown in Figure 16.



Figure 16. The fully-dense additive components with AFSD [62].

The AFSD process is used to repair lightweight structure parts by replacing the cracked or corroded material with the deposited material [63]. Martin et al. [36,64] repaired the groove in AA6061-T651 and cast Al-1.4Si-1.1Cu-1.5Mg-2.1Zn by adopting the AFSD process of 6061-T6 feedstock, as shown in Figure 17. In addition, Martin et al. [13] explored the possibility of repairing AISI 4340 steel with AISI 316L based on the AFSD process, including groove-filling and surface deposition. Griffiths et al. [12] achieved the groove and cylindrical through-holes repair of AA7075. Moreover, it should be mentioned that the width of the feeding rod was less than that of the groove. MELD explored the wider applications of AFSD, as shown in Figure 18.

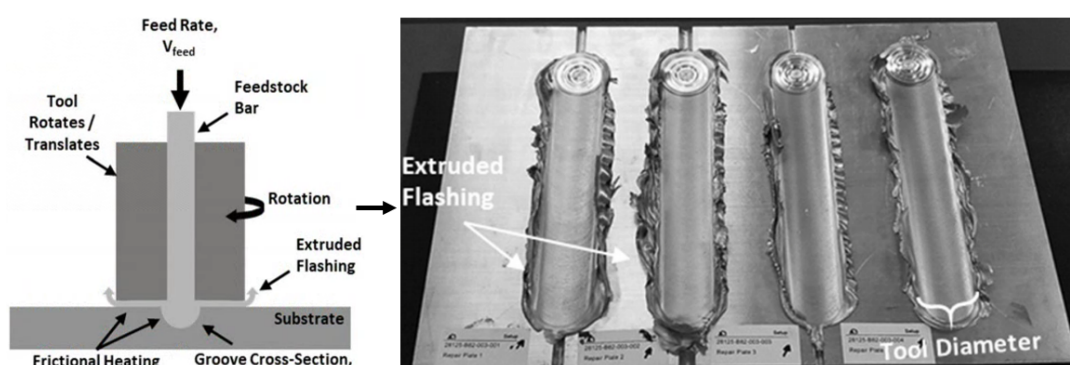


Figure 17. The schematic and the repaired result of AA6061-T651 [36].

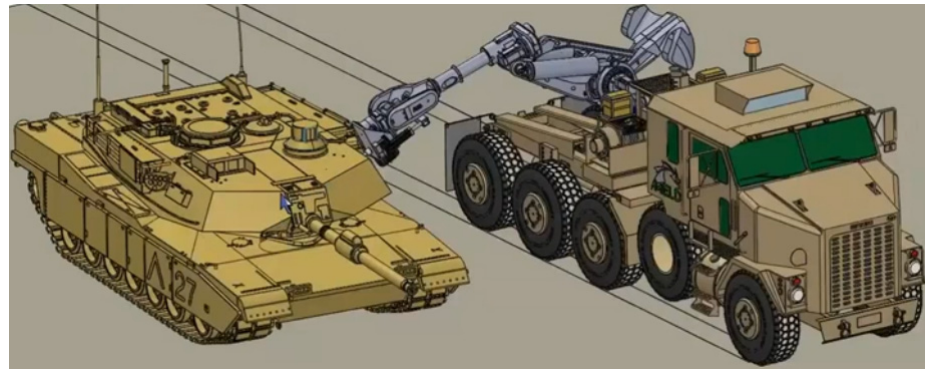


Figure 18. The possible repairing application of AFSD on the tank [62].

Another engineering application is the solid-state recycling of AFSD, as shown in Figure 19. Babaniaris et al. [37] consolidated the AA6063 swarf into rod feedstock via hot extrusion and then deposited the extruded rod by AFSD process. By the post-deposition heat treatment, the deposited AA6063 has wrought-like properties. Without consolidation, Jordan et al. [11] achieved the direct recycling of AA5083-H131 chips based on the AFSD process. Similar recycling was also achieved on Ti6Al4V chips.

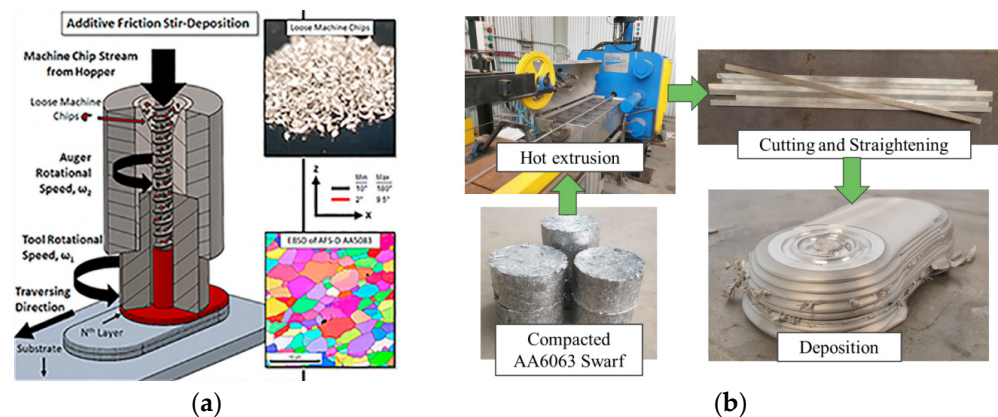


Figure 19. Different solid-state recycling processes. (a) Direct recycling of chips [11]. (b) Multi-step recycling of swarf [37].

Some researchers have explored the application of AFSD to surface coating. Gandra et al. [65] deposited the AA6082/SiC coating surface composite with a consumable rod. In addition, MELD explored the deposition of Cu on tantalum and niobium at different positions, as shown in Figure 20.

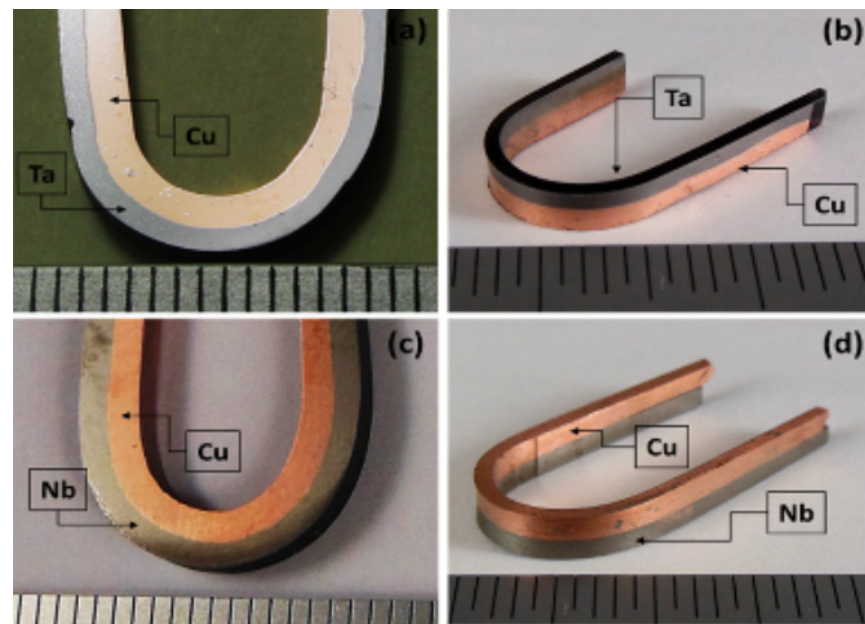


Figure 20. Copper coating on different materials. (a,b) On tantalum. (c,d) On niobium [66].

5. Perspective

5.1. The Characterization Method and Unified Constitutive Model under Severe Transient Thermo-Mechanical Conditions

AFSD is a process of multiple deformation combinations under elevated temperature, including compression, torsion, and shear. Moreover, the strain rate and temperature experience rapid change, which makes the transient thermo-mechanical flow behavior become more complicated. The microstructure changes dramatically during AFSD, including the grain size, phase transition, second phase, etc., which has a significant effect on material flow behavior. Research on the above can enrich and develop theories on plastic-forming under the coupling of large strain, multiple deformation mode, and elevated temperature. Meanwhile, the finite element simulation needs precise constitutive models to predict the flow behavior and study the deformation mechanism during the AFSD process. The corresponding characterization method under complex loading paths and elevated temperature also needs further development to establish a precise constitutive model.

5.2. The Post-Deposition Heat Treatment

During the AFSD process, for the precipitation hardenable alloy, the precipitate may dissolve under the function of high temperature, which may decrease material strength. Meanwhile, the new precipitate can form and grow. For the cold-worked hardenable alloy, the accumulated dislocation may annihilate due to the dynamic recrystallization and dynamic recovery, which may decrease the material strength. In addition, due to different deformation strain history and thermal recycling history, there is the microstructure gradient and mechanical property gradient in the deposited zone, which affects material service performance. Therefore, there is a requirement for post-deposition heat treatment to improve material strength and performance consistency. Moreover, whether the traditional heat treatment system is suitable for the deposited material needs further study.

5.3. The Composite Manufacturing of Additive and Reduced Process

There is no melting and rapid solidification process during the AFSD process, which can avoid solidification deformation. Meanwhile, the dynamic recrystallization makes the accumulated dislocation annihilate, which can decrease the residual stress. In addition, the AFSD has a high deposition rate, such as Al up to 13.6 kg/h, which makes the ASFD suitable for producing the large part. However, the part accuracy is low due to the restriction of the

AFSD process, while the machining has high accuracy. Therefore, based on the advantage of the above-mentioned high deposition rate, low residual stress, and high machining accuracy, it is worth exploring the composite manufacturing process of additive and reduced process.

5.4. A Systematic Study on the AFSD Process

Before conducting AFSD, metal powder and rods are often used as the raw material for the AFSD process. The powder size, bar grain size, and bar heat treatment temper often significantly influence the mechanical properties of deposited material. During the AFSD process, besides the mentioned parameters in Table 2, temperature control also plays an important role in the deposition quality. High deposition temperature leads to obvious grain growth, while low deposition temperature leads to insufficient plastic flow. Moreover, different thermal recycling histories at each layer lead to non-uniform mechanical property distribution. Therefore, how to control temperature evolution is a vital question during the AFSD process. After conducting the AFSD process, microhardness and tensile tension tests are often used to measure the deposition quality. However, it is not enough to judge the service performance of parts. Therefore, there is still a lack of a systematic study on the AFSD process, from the raw materials to the service performance.

6. Conclusions

As a new solid-state-based additive manufacturing technology, the AFSD process can deposit material under melting temperature, solving some severe issues related to laser- or electric beam-based AM. Moreover, this additive method can be used in a wide range of materials and engineering applications. Some critical conclusions are summarized as follows:

1. The primary mechanism of AFSD is mainly related to temperature and plastic deformation. Different high-temperature deformation behaviors lead to different heat generation mechanisms and deformation mechanisms for different materials.
2. Due to high temperature and large plastic deformation, dynamic recrystallization is a common characteristic of different deposition materials. Meanwhile, it is accompanied by grain growth, phase transition, precipitate evolution, etc. The above characters may reduce or improve the mechanical properties. Due to complex microstructure evolution, the corresponding characterization method and unified constitutive model under severe transient thermo-mechanical conditions need further study.
3. Post-deposition heat treatment is a valid method to improve material performance, including strength and performance uniformity, especially for materials with degraded performance after deposition. The corresponding heat treatment system needs further study.
4. The AFSD process can be used in different situations, including producing large parts, surface coating, repairing large parts, etc. However, AFSD has the limitation of low manufacturing accuracy and low flexibility. Therefore, the composite manufacturing of additive and reduced processes is a trend to produce high-accuracy parts.

Author Contributions: Conceptualization, H.D. and X.L. (Xiaoqiang Li); resources, X.L. (Xiaoqiang Li); writing—original draft preparation, H.D., K.X. and Z.Z. (Zhenyu Zang); writing—review and editing, X.L. (Xiaoqiang Li), W.X., Z.Z. (Zongjiang Zhang) and Y.L.; supervision, X.L. (Xin Liu); project administration, X.L. (Xiaoqiang Li); funding acquisition, X.L. (Xiaoqiang Li). All authors have read and agreed to the published version of the manuscript.

Funding: This work was supported by the Fundamental Research Funds for the Central Universities (YWF-22-L-504).

Institutional Review Board Statement: Not applicable.

Informed Consent Statement: Not applicable.

Conflicts of Interest: The authors declare no conflict of interest.

References

1. Frazier, W.E. Metal additive manufacturing: A review. *J. Mater. Eng. Perform.* **2014**, *23*, 1917–1928. [CrossRef]
2. Sames, W.J.; List, F.; Pannala, S.; Dehoff, R.R.; Babu, S.S. The metallurgy and processing science of metal additive manufacturing. *Int. Mater. Rev.* **2016**, *61*, 315–360. [CrossRef]
3. Agrawal, P.; Thapliyal, S.; Nene, S.; Mishra, R.; McWilliams, B.; Cho, K. Excellent strength-ductility synergy in metastable high entropy alloy by laser powder bed additive manufacturing. *Addit. Manuf.* **2020**, *32*, 101098. [CrossRef]
4. Liu, S.; Bor, T.; Van der Stelt, A.; Geijselaers, H.; Kwakernaak, C.; Kooijman, A.; Mol, J.; Akkerman, R.; Van Den Boogaard, A. Friction surface cladding: An exploratory study of a new solid state cladding process. *J. Mater. Process. Technol.* **2016**, *229*, 769–784. [CrossRef]
5. Van Der Stelt, A.; Bor, T.C.; Geijselaers, H.J.; Akkerman, R.; van den Boogaard, A.H. Cladding of advanced Al alloys employing friction stir welding. *Key Eng. Mater.* **2013**, *554*, 1014–1021.
6. Perry, M.E.; Griffiths, R.J.; Garcia, D.; Sietins, J.M.; Zhu, Y.; Hang, Z.Y. Morphological and microstructural investigation of the non-planar interface formed in solid-state metal additive manufacturing by additive friction stir deposition. *Addit. Manuf.* **2020**, *35*, 101293. [CrossRef]
7. Mason, C.; Rodriguez, R.I.; Avery, D.Z.; Phillips, B.J.; Bernarding, B.P.; Williams, M.; Cobbs, S.D.; Jordon, J.B.; Allison, P. Process-structure-property relations for as-deposited solid-state additively manufactured high-strength aluminum alloy. *Addit. Manuf.* **2021**, *40*, 101879. [CrossRef]
8. Calvert, J.R. Microstructure and Mechanical Properties of WE43 Alloy Produced via Additive Friction Stir Technology. Master's Thesis, Virginia Tech, Blacksburg, VA, USA, 2015.
9. Jha, K.K.; Kesharwani, R.; Imam, M. Microstructural and micro-hardness study on the fabricated Al 5083-O/6061-T6/7075-T6 gradient composite component via a novel route of friction stir additive manufacturing. *Mater. Today Proc.* **2022**, *56*, 819–825.
10. Griffiths, R.J.; Perry, M.E.; Sietins, J.M.; Zhu, Y.; Hardwick, N.; Cox, C.D.; Rauch, H.A.; Yu, H.Z. A perspective on solid-state additive manufacturing of aluminum matrix composites using MELD. *J. Mater. Eng. Perform.* **2019**, *28*, 648–656. [CrossRef]
11. Jordon, J.; Allison, P.; Phillips, B.; Avery, D.; Kinser, R.; Brewer, L.; Cox, C.; Doherty, K. Direct recycling of machine chips through a novel solid-state additive manufacturing process. *Mater. Des.* **2020**, *193*, 108850. [CrossRef]
12. Griffiths, R.J.; Petersen, D.T.; Garcia, D.; Yu, H.Z. Additive friction stir-enabled solid-state additive manufacturing for the repair of 7075 aluminum alloy. *Appl. Sci.* **2019**, *9*, 3486. [CrossRef]
13. Martin, L.P.; Luccitti, A.; Walluk, M. Evaluation of Additive Friction Stir Deposition of AISI 316L For Repairing Surface Material Loss in AISI 4340. 2022. Available online: <https://assets.researchsquare.com/files/rs-1214920/v1/1949905c-1540-44c7-bd10-47b5598123a2.pdf?c=1641484869> (accessed on 20 July 2022).
14. Khodabakhshi, F.; Gerlich, A. Potentials and strategies of solid-state additive friction-stir manufacturing technology: A critical review. *J. Manuf. Process.* **2018**, *36*, 77–92. [CrossRef]
15. Srivastava, A.K.; Kumar, N.; Dixit, A.R. Friction stir additive manufacturing—An innovative tool to enhance mechanical and microstructural properties. *Mater. Sci. Eng. B* **2021**, *263*, 114832. [CrossRef]
16. Srivastava, A.K.; Dixit, V.; Rai, A.K.; Sharma, S.; Sharma, A.; Srivastava, V.S. Study of microstructural and mechanical properties of the component produced by friction stir additive manufacturing (FSAM)—A review. *Mater. Today Proc.* **2021**, *47*, 4142–4147. [CrossRef]
17. Srivastava, M.; Rathee, S.; Maheshwari, S.; Noor Siddiquee, A.; Kundra, T. A review on recent progress in solid state friction based metal additive manufacturing: Friction stir additive techniques. *Crit. Rev. Solid State Mater. Sci.* **2019**, *44*, 345–377. [CrossRef]
18. Available online: <https://www.mouldu.com/uploadfile/2019/0618/20190618112127861.png> (accessed on 20 July 2022).
19. Elfshawy, E.; Ahmed, M.; El-Sayed Seleman, M. Additive manufacturing of aluminum using friction stir deposition. In *TMS 2020 149th Annual Meeting & Exhibition Supplemental Proceedings*; The Minerals, Metals & Materials Series; Springer: Cham, Switzerland, 2020; pp. 227–238. [CrossRef]
20. Mukhopadhyay, A.; Saha, P. Mechanical and microstructural characterization of aluminium powder deposit made by friction stir based additive manufacturing. *J. Mater. Process. Technol.* **2020**, *281*, 116648. [CrossRef]
21. Karthik, G.; Ram, G.J.; Kottada, R.S. Friction deposition of titanium particle reinforced aluminum matrix composites. *Mater. Sci. Eng. A* **2016**, *653*, 71–83. [CrossRef]
22. Chaudhary, B.; Jain, N.K.; Murugesan, J.; Patel, V. Exploring temperature-controlled friction stir powder additive manufacturing process for multi-layer deposition of aluminum alloys. *J. Mater. Res. Technol.* **2022**, *20*, 260–268. [CrossRef]
23. El-Sayed Seleman, M.M.; Ataya, S.; Ahmed, M.M.; Hassan, A.M.; Latief, F.H.; Hajlaoui, K.; El-Nikhaily, A.E.; Habba, M.I. The Additive Manufacturing of Aluminum Matrix Nano Al₂O₃ Composites Produced via Friction Stir Deposition Using Different Initial Material Conditions. *Materials* **2022**, *15*, 2926. [CrossRef]
24. Chaudhary, B.; Jain, N.K.; Murugesan, J. Development of friction stir powder deposition process for repairing of aerospace-grade aluminum alloys. *CIRP J. Manuf. Sci. Technol.* **2022**, *38*, 252–267. [CrossRef]
25. Gopan, V.; Wins, K.L.D.; Surendran, A. Innovative potential of additive friction stir deposition among current laser based metal additive manufacturing processes: A review. *CIRP J. Manuf. Sci. Technol.* **2021**, *32*, 228–248. [CrossRef]
26. Derazkola, H.A.; Khodabakhshi, F.; Gerlich, A. Fabrication of a nanostructured high strength steel tube by friction-forging tubular additive manufacturing (FFTAM) technology. *J. Manuf. Process.* **2020**, *58*, 724–735. [CrossRef]

27. Garcia, D.; Hartley, W.D.; Rauch, H.A.; Griffiths, R.J.; Wang, R.; Kong, Z.J.; Zhu, Y.; Hang, Z.Y. In situ investigation into temperature evolution and heat generation during additive friction stir deposition: A comparative study of Cu and Al-Mg-Si. *Addit. Manuf.* **2020**, *34*, 101386. [CrossRef]
28. Joshi, S.S.; Sharma, S.; Radhakrishnan, M.; Pantawane, M.V.; Patil, S.M.; Jin, Y.; Yang, T.; Riley, D.A.; Banerjee, R.; Dahotre, N.B. A multi modal approach to microstructure evolution and mechanical response of additive friction stir deposited AZ31B Mg alloy. *Sci. Rep.* **2022**, *12*, 13234. [CrossRef] [PubMed]
29. Mishra, R.S.; Ma, Z. Friction stir welding and processing. *Mater. Sci. Eng. R Rep.* **2005**, *50*, 1–78. [CrossRef]
30. Perry, M.E.; Rauch, H.A.; Griffiths, R.J.; Garcia, D.; Sietins, J.M.; Zhu, Y.; Zhu, Y.; Hang, Z.Y. Tracing plastic deformation path and concurrent grain refinement during additive friction stir deposition. *Materialia* **2021**, *18*, 101159. [CrossRef]
31. McNelley, T.; Swaminathan, S.; Su, J. Recrystallization mechanisms during friction stir welding/processing of aluminum alloys. *Scr. Mater.* **2008**, *58*, 349–354. [CrossRef]
32. Sakai, T.; Belyakov, A.; Kaibyshev, R.; Miura, H.; Jonas, J.J. Dynamic and post-dynamic recrystallization under hot, cold and severe plastic deformation conditions. *Prog. Mater. Sci.* **2014**, *60*, 130–207. [CrossRef]
33. Hartley, W.D.; Garcia, D.; Yoder, J.K.; Poczatek, E.; Forsmark, J.H.; Luckey, S.G.; Dillard, D.A.; Hang, Z.Y. Solid-state cladding on thin automotive sheet metals enabled by additive friction stir deposition. *J. Mater. Process. Technol.* **2021**, *291*, 117045. [CrossRef]
34. Beck, S.; Rutherford, B.; Avery, D.; Phillips, B.; Rao, H.; Rekha, M.; Brewer, L.; Allison, P.; Jordon, J. The effect of solutionizing and artificial aging on the microstructure and mechanical properties in solid-state additive manufacturing of precipitation hardened Al–Mg–Si alloy. *Mater. Sci. Eng. A* **2021**, *819*, 141351. [CrossRef]
35. Joshi, S.S.; Patil, S.M.; Mazumder, S.; Sharma, S.; Riley, D.A.; Dowden, S.; Banerjee, R.; Dahotre, N.B. Additive friction stir deposition of AZ31B magnesium alloy. *J. Magnes. Alloys* **2022**. [CrossRef]
36. Martin, L.P.; Luccitti, A.; Walluk, M. Repair of aluminum 6061 plate by additive friction stir deposition. *Int. J. Adv. Manuf. Technol.* **2022**, *118*, 759–773. [CrossRef]
37. Babaniaris, S.; Jiang, L.; Varma, R.K.; Farabi, E.; Dorin, T.; Barnett, M.; Fabijanac, D. Solid-State Recycling of AA6063 Swarf Using Additive Friction Stir Deposition. Available online: <https://ssrn.com/abstract=4156727> (accessed on 20 July 2022).
38. Rivera, O.; Allison, P.; Jordon, J.; Rodriguez, O.; Brewer, L.; McClelland, Z.; Whittington, W.; Francis, D.; Su, J.; Martens, R. Microstructures and mechanical behavior of Inconel 625 fabricated by solid-state additive manufacturing. *Mater. Sci. Eng. A* **2017**, *694*, 1–9. [CrossRef]
39. Priedeman, J.L.; Phillips, B.J.; Lopez, J.J.; Tucker Roper, B.E.; Hornbuckle, B.C.; Darling, K.A.; Jordon, J.B.; Allison, P.G.; Thompson, G.B. Microstructure development in additive friction stir-deposited Cu. *Metals* **2020**, *10*, 1538. [CrossRef]
40. Agrawal, P.; Haridas, R.S.; Yadav, S.; Thapliyal, S.; Gaddam, S.; Verma, R.; Mishra, R.S. Processing-structure-property correlation in additive friction stir deposited Ti-6Al-4V alloy from recycled metal chips. *Addit. Manuf.* **2021**, *47*, 102259. [CrossRef]
41. Polar, A.; Indacochea, J. Microstructural assessment of copper friction stir welds. *J. Manuf. Sci. Eng.* **2009**, *131*, 031012. [CrossRef]
42. Phillips, B.; Avery, D.; Liu, T.; Rodriguez, O.; Mason, C.; Jordon, J.; Brewer, L.; Allison, P. Microstructure-deformation relationship of additive friction stir-deposition Al–Mg–Si. *Materialia* **2019**, *7*, 100387. [CrossRef]
43. Farabi, E.; Babaniaris, S.; Barnett, M.R.; Fabijanac, D.M. Microstructure and mechanical properties of Ti6Al4V alloys fabricated by additive friction stir deposition. *Addit. Manuf. Lett.* **2022**, *2*, 100034. [CrossRef]
44. Rivera, O.; Allison, P.; Brewer, L.; Rodriguez, O.; Jordon, J.; Liu, T.; Whittington, W.; Martens, R.; McClelland, Z.; Mason, C. Influence of texture and grain refinement on the mechanical behavior of AA2219 fabricated by high shear solid state material deposition. *Mater. Sci. Eng. A* **2018**, *724*, 547–558. [CrossRef]
45. Simar, A.; Bréchet, Y.; De Meester, B.; Denquin, A.; Gallais, C.; Pardoën, T. Integrated modeling of friction stir welding of 6xxx series Al alloys: Process, microstructure and properties. *Prog. Mater. Sci.* **2012**, *57*, 95–183. [CrossRef]
46. Trueba Jr, L.; Heredia, G.; Rybicki, D.; Johannes, L.B. Effect of tool shoulder features on defects and tensile properties of friction stir welded aluminum 6061-T6. *J. Mater. Process. Technol.* **2015**, *219*, 271–277. [CrossRef]
47. Avery, D.; Phillips, B.; Mason, C.; Palermo, M.; Williams, M.; Cleek, C.; Rodriguez, O.; Allison, P.; Jordon, J. Influence of grain refinement and microstructure on fatigue behavior for solid-state additively manufactured Al-Zn-Mg-Cu alloy. *Metall. Mater. Trans. A* **2020**, *51*, 2778–2795. [CrossRef]
48. Phillips, B.; Mason, C.; Beck, S.; Avery, D.; Doherty, K.; Allison, P.; Jordon, J. Effect of parallel deposition path and interface material flow on resulting microstructure and tensile behavior of Al-Mg-Si alloy fabricated by additive friction stir deposition. *J. Mater. Process. Technol.* **2021**, *295*, 117169. [CrossRef]
49. Robinson, T.W.; Williams, M.; Rao, H.; Kinser, R.P.; Allison, P.; Jordon, J. Microstructural and Mechanical Properties of a Solid-State Additive Manufactured Magnesium Alloy. *J. Manuf. Sci. Eng.* **2022**, *144*, 061013. [CrossRef]
50. Williams, M.; Robinson, T.; Williamson, C.; Kinser, R.; Ashmore, N.; Allison, P.; Jordon, J. Elucidating the effect of additive friction stir deposition on the resulting microstructure and mechanical properties of magnesium alloy we43. *Metals* **2021**, *11*, 1739. [CrossRef]
51. Anderson-Wedge, K.; Avery, D.; Daniewicz, S.; Sowards, J.; Allison, P.; Jordon, J.; Amaro, R. Characterization of the fatigue behavior of additive friction stir-deposition AA2219. *Int. J. Fatigue* **2021**, *142*, 105951. [CrossRef]
52. Song, K.H.; Nakata, K. Mechanical properties of friction-stir-welded Inconel 625 alloy. *Mater. Trans.* **2009**, *50*, 0909070891. [CrossRef]
53. Ye, F.; Fujii, H.; Tsumura, T.; Nakata, K. Friction stir welding of Inconel alloy 600. *J. Mater. Sci.* **2006**, *41*, 5376–5379. [CrossRef]

54. Avery, D.; Rivera, O.; Mason, C.; Phillips, B.; Jordon, J.; Su, J.; Hardwick, N.; Allison, P. Fatigue behavior of solid-state additive manufactured inconel 625. *JOM* **2018**, *70*, 2475–2484. [[CrossRef](#)]
55. Tan, Z.; Li, J.; Zhang, Z. Experimental and numerical studies on fabrication of nanoparticle reinforced aluminum matrix composites by friction stir additive manufacturing. *J. Mater. Res. Technol.* **2021**, *12*, 1898–1912. [[CrossRef](#)]
56. Avery, D.Z.; Cleek, C.; Phillips, B.J.; Rekha, M.; Kinser, R.P.; Rao, H.; Brewer, L.; Allison, P.; Jordon, J. Evaluation of Microstructure and Mechanical Properties of Al-Zn-Mg-Cu Alloy Repaired via Additive Friction Stir Deposition. *J. Eng. Mater. Technol.* **2022**, *144*, 031003. [[CrossRef](#)]
57. Rohatgi, N. Analysis of Friction Stir Additive Manufacturing and Friction Stir Welding of al6061-t6 via Numerical Modeling and Experiments. Master's Thesis, Purdue University, West Lafayette, IN, USA, 2020.
58. Stubblefield, G.; Fraser, K.; Phillips, B.; Jordon, J.; Allison, P. A meshfree computational framework for the numerical simulation of the solid-state additive manufacturing process, additive friction stir-deposition (AFS-D). *Mater. Des.* **2021**, *202*, 109514. [[CrossRef](#)]
59. Yang, H. Numerical Simulation of the Temperature and Stress State on the Additive Friction Stir with the Smoothed Particle Hydrodynamics Method. *Strength Mater.* **2020**, *52*, 24–31. [[CrossRef](#)]
60. Stubblefield, G.G. Smoothed Particle Hydrodynamic Modeling of Solid State Additively Manufactured Aluminum Alloys. Ph.D. Thesis, The University of Alabama, Tuscaloosa, AL, USA, 2021.
61. Lauvray, A.; Poulhaon, F.; Michaud, P.; Joyot, P.; Duc, E. Additive Friction Stir Manufacturing Process: Interest in Understanding Thermal Phenomena and Numerical Modeling of the Temperature Rise Phase. In Proceedings of the Innovative Manufacturing Systems and Processes, Prague, Czechia, 6–7 September 2021.
62. Meld Manufacturing. Available online: <http://meldmanufacturing.com> (accessed on 20 July 2022).
63. Zuo, Y.-Y.; Liu, H.; Gong, P.; Ji, S.-D.; Wu, B.-S. Radial additive friction stir repairing of mechanical hole out of dimension tolerance of AZ31 magnesium alloy assisted by stationary shoulder: Process and mechanical properties. *Acta Metall. Sin.* **2021**, *34*, 1345–1360. [[CrossRef](#)]
64. Peter Martin, L.; Luccitti, A.; Walluk, M. Evaluation of Additive Friction Stir Deposition for the Repair of Cast Al-1.4 Si-1.1 Cu-1.5 Mg-2.1 Zn. *J. Manuf. Sci. Eng.* **2022**, *144*, 061006. [[CrossRef](#)]
65. Gandra, J.; Vigarinho, P.; Pereira, D.; Miranda, R.; Velhinho, A.; Vilaça, P. Wear characterization of functionally graded Al-SiC composite coatings produced by friction surfacing. *Mater. Des. (1980–2015)* **2013**, *52*, 373–383. [[CrossRef](#)]
66. Use Meld to Coat. Available online: <http://meldmanufacturing.com/coat/> (accessed on 20 July 2022).